AIAA JOURNAL
Vol. 40, No. 1, January 2002

Fuzzy Finite Element Method for Frequency Response Function Analysis of Uncertain Structures

David Moens* and Dirk Vandepitte†
Katholieke Universiteit Leuven, 3001 Heverlee, Belgium

A concept is presented for incorporating fuzzy uncertainties in dynamic finite element analyses of uncertain structures. The objective is twofold. The first goal is to clarify and extend the classical fuzzy finite element (FFE) method as it was introduced for static analyses. The shortcomings of the classical approach are described, and an extension to a generalized approach is proposed. This generalized approach is proven to be a more realistic and therefore more reliable concept for taking uncertainty into account. The second goal is to illustrate the applicability of the method for dynamic analyses. The classical and the generalized approach are compared using an eigenvalue analysis of a simple numerical example. The FFE method is also applied to the calculation of the total envelope frequency response function (FRF) using the modal superposition principle. This method requires safe approximations of the individual mode envelope frequency response functions. For this purpose a number of safe approximate optimization strategies are introduced. The numerical example shows that useful results are obtained using this FFE approach for FRF calculations.

Nomenclature

A	=	vector or matrix
$\boldsymbol{A}$	=	interval vector or matrix
a	=	scalar
$\boldsymbol{a}$	=	interval scalar
$\bar{a}, \underline{a}$	=	upper and lower bounds on $\boldsymbol{a}$, respectively
$\overline{\bar{a}}, \underline{\underline{a}}$	=	conservative (high and low) approximation of $\bar{a}$ and $\underline{a}$, respectively
$\tilde{a}$	=	fuzzy variable
$\underline{\overline{f(\omega)}}_{\beta}$	=	envelope of function f in ω domain considering the uncertain parameters β
$\overline{\overline{f(\omega)}}$	=	conservative approximation of $\underline{\overline{f(\omega)}}_{\beta}$
$\mu_{\tilde{a}}(x)$	=	membership function of the fuzzy variable defined in x

I. Introduction

THE finite element (FE) method is a very popular tool for both static and dynamic structural analysis. The ability to predict the behavior of a structure under static or dynamic loads is not only of great scientific value, it is also very useful from an economical point of view. A reliable FE analysis could make prototype production and testing obsolete and therefore significantly reduce the associated design validation cost. Unfortunately, it sometimes is very difficult to ensure the reliability of the result of an FE analysis for realistic mechanical structures that are not precisely defined. A number of errors incorporated in the analysis could cause the result to be erroneous and therefore unreliable. These errors are classified here in two classes: the theoretical error and the practical error.

There are two kinds of theoretical errors. The first is the discretization error, which is caused by the finite representation of reality. This error will always be present to some extent in the result of an FE analysis. It can be reduced by increasing the model size. For realistic models, this significantly increases the computational cost of the analysis. The second kind of theoretical error is caused by the underlying mathematical descriptions of the analyzed physical phenomena. The partial differential equations that describe the structural behavior are based on assumptions of which the validity is not always ensured. A more important error is introduced through the FE shape functions, which are simple polynomial functions and often do not obey the governing differential equations. No precautions can be taken to reduce the error resulting from either the differential equations nor the shape functions because both are inherent to the FE methodology.

The practical error is caused by the inaccuracy of the FE model parameters. Unlike the former theoretical ones, the practical error in an FE model vanishes completely if perfect values of all physical properties (material properties, connections, geometry...) are available. Because this is never the case, one should always be aware of the error introduced by this incomplete knowledge. This paper focuses only on the effect of the practical error.

Despite the uncertainties just mentioned, FE analyses are in many cases useful to gain knowledge of the dynamic behavior of a structure while it is still in the design phase. However, it is not safe to base design validation on these deterministic analyses. Even if the design is completely defined, production inaccuracy and design tolerances introduce variability, resulting in a scatter of possible results for the analysis. Reliable validation can only be based on an analysis, which takes into account the uncertainties that are causing this variability. A number of stochastic methods have been introduced to address this problem. These methods are able to calculate the exact stochastic description of the uncertainty on the result of dynamical analyses if the stochastic description of the uncertainties on the model are known. A number of FE techniques were developed[1,2] for this purpose. The most straightforward and most popular tool is the Monte Carlo simulation technique. Because this technique necessitates a large number of samples, it is often computationally very expensive for realistic models. Special techniques have to be developed to reduce the amount of computational effort for each sample.[3] The most restricting assumption of the stochastic methods however is the exact knowledge of the stochastic properties of each uncertainty in the model. Especially in an early design stage, not every uncertainty can be formulated in a stochastic manner. Elishakoff[4] showed that using estimations for statistical data is unsafe for design validation purposes. The stochastic result for those cases is unreliable and might lead to false conclusions. However, it is common practice to use a stochastic approach for reliability considerations. As such, sufficiently large safety factors are mandatory.

Received 6 February 2001; revision received 15 June 2001; accepted for publication 4 July 2001.

*Research Assistant of the Fund for Scientific Research—Flanders, Belgium, Department of Mechanical Engineering, PMA Division, Celestijnenlaan 300B.

†Professor, Department of Mechanical Engineering, PMA Division, Celestijnenlaan 300B. Member AIAA.

The fuzzy finite element (FFE) method[5] addresses the problems of the Monte Carlo simulation and other stochastic techniques already mentioned. It is capable of handling linguistic and therefore more realistic design uncertainty descriptions. Absence of knowledge does not require a stochastic probability estimation. Furthermore, its underlying mathematical procedures are based on worst-case scenarios, which enables a simplified nonstochastic approach for reliability considerations. Using the worst case result of an FFE analysis for design validation in principle requires no safety factor. Therefore, if an FFE approach would be efficiently applicable on dynamic analysis used for design validation it would be a valuable alternative for the existing stochastic techniques.

It is the aim of this paper to illustrate the applicability of the FFE method for dynamic design validation. A method for the calculation of fuzzy frequency response functions (FRF) of uncertain structures is presented. The procedure calculates a fuzzy description of the envelope on the response function starting from fuzzy uncertainties on the input model, using the FFE methodology.

II. FFE Method

This section first presents a short overview of the basic concepts of the theory of fuzzy logic introduced by Zadeh.[6] Further, it describes the classical FFE analysis as described by Rao and Sawyer.[5] This section shows that the result of the classical FFE approach is not a realistic description of the uncertainty on the analyzed phenomenon. Therefore, the classical approach is extended to a more realistic generalized FFE approach. Both approaches are compared for an eigenvalue analysis of a simple numerical example. Finally, computational aspects of the classical and generalized approach are discussed.

A. Fuzzy Logic

1. Membership Function

A fuzzy variable is defined as a member of a fuzzy subset of a domain. The membership function describes the grade of membership to this fuzzy subset of each element in the domain. For a fuzzy variable $\tilde{x}$ the membership function is defined as $\mu_{\tilde{x}}(x)$ for all x that belong to the domain $\mathcal{X}$. If $\mu_{\tilde{x}}(x) = 1$, x is definitely a member of the subset $\tilde{x}$. If $\mu_{\tilde{x}}(x) = 0$, x is definitely not a member of the subset $\tilde{x}$. For every x with $0 < \mu_{\tilde{x}}(x) < 1$, the membership is not certain. Figure 1 shows typical triangular membership functions.

Zadeh[7] introduced the theory of fuzzy sets as a basis for reasoning with possibility. From this point of view, the membership function is considered as a possibility distribution function, providing information on the values that the described quantity can adopt. More generally, the possibility is defined as a subjective measure that expresses the degree to which a person considers that an event can occur. As such, it provides a system of defining intermediate possibilities between strictly impossible and strictly possible events. The choice of the possibility distribution of a quantity of which no statistical data are available is subjective and can only be based on expert opinion. On the other hand, a number of methods exist to derive a possibility distribution corresponding to a known probability density function.[8,9] However, apart from the probability distribution, these conversion techniques always rely on some sort of subjective judgement. This is why a possibilistic analysis can only be interpreted in reference to the input possibilities. This will be further clarified in the next section.

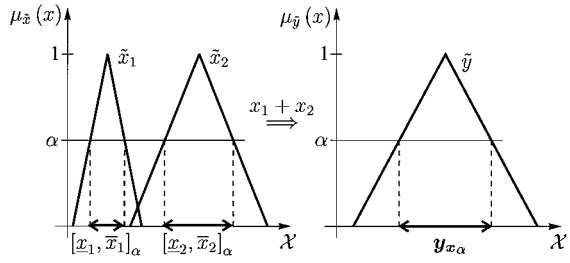

Fig. 1 Calculation of the result of the function $\mathcal{F}(x_1, x_2) = x_1 + x_2$ by subdivision of the range of the membership function.

2. Fuzzy Arithmetic

Different procedures exist for the calculation of results of functions of fuzzy variables. The most widely known and applied concept is fuzzy arithmetic. This concept consists of a sequence of max-min operations on a numeric representation of the membership functions of the input variables. Because the size of the representation of the fuzzy result grows with every operation, this concept is rarely applied in numerical computations. A different technique using α sublevels has been introduced. In this technique the fuzzy solution is converted into a set of interval solutions. This is done by subdividing the range of the membership function into a number of α sublevels. At each sublevel an interval analysis is performed using the bounds of all fuzzy input parameters at the particular level. Combining all results of the interval analyses for all of the α sublevels results in the membership function for the result of the operation.

The core problem in the calculation of the result of a function of fuzzy variables is the calculation of the result of that function in interval arithmetic. For a function of n fuzzy variables $\mathcal{F}(\tilde{x}_1, \tilde{x}_2, \ldots, \tilde{x}_n)$, the result is calculated at each α sublevel from the solution set $\boldsymbol{y}_{x_\alpha}$ defined as

$$\boldsymbol{y}_{x_\alpha} = \{y \mid (\exists x_i \in \boldsymbol{x}_{i_\alpha}, i = 1, 2, \ldots n)(y = \mathcal{F}(x_1, x_2, \ldots, x_n))\} \quad (1)$$

with $\boldsymbol{x}_{i_\alpha}$ describing the interval of the variable x_i at level α. Finally, the fuzzy solution is assembled from the resulting intervals at each sublevel, repeating this procedure for a number of α sublevels. Figure 1 clarifies this procedure for a function $\mathcal{F}$ representing an addition of two triangular fuzzy variables. This technique guarantees a constant size of the representation of the fuzzy result of each intermediate step during computation. Another advantage is that the calculation of a fuzzy function can be optimized to a tradeoff between computational effort and accuracy by selecting the number of α sublevels.

It is now clear that the fuzzy analysis in this case is a sort of large-scale sensitivity analysis of the combined effect of design variables and uncertainties on design requirements. It enables the analyst to calculate the α level and corresponding design variable ranges for which the design meets the requirements with a certain degree of possibility. This means that the interpretation of the result of the analysis is only meaningful by referring to the considered input possibility distributions. A different possibility distribution for the design variables will yield a different possibility distribution of the analysis result and consequently also different allowable ranges for the design variables. The design based on this analysis however is equally safe. As such, the possibility distribution for a designer is merely a useful tool to control the allowable range for the uncertainties than an absolute quality measure.

B. Classical FFE Method

This part discusses the classical FFE method as introduced by Rao and Sawyer in Ref. 5. The classical FFE method is based on a deterministic FE analysis. It consists of three major parts: the fuzzy model definition, the assembly of the fuzzy system matrices, and the calculation of the results of the analysis.

1. Fuzzy Model Definition

The definition of a FE model consists of the definition and discretization of the geometry, definition of the material properties, definition of the constraints and loads, and the specification of the result request. Depending on the kind of the intended analysis, some additional inputs are required. Some of the inputs are always present in an uncertain nature. The uncertainty on the geometry, material properties, and constraints either results from design uncertainties or is caused by manufacturing variability. Uncertainty on the applied loads might result from imprecise reference loading conditions. All of these uncertainties should be described by membership functions. If a stochastic description of an uncertain value is available, an equivalent membership function is introduced for this value. Crisp membership functions describe certain values.

2. Assembly of the Fuzzy System Matrices

The classical FFE method starts from the fuzzy model definition for the assembly of the system matrices that are necessary for the FE analysis. The dynamic system matrices are assembled from the element stiffness, mass and damping matrices K^e, M^e, and C^e using

$$K = \bigcup K^e \tag{2}$$

$$M = \bigcup M^e \tag{3}$$

$$C = \bigcup C^e \tag{4}$$

with $\bigcup$ representing the assembly over all of the elements of the FE model. The element matrices are calculated using

$$K^e = \int_{V^e} B^T D B \, \mathrm{d}V \tag{5}$$

$$M^e = \int_{V^e} N^T \rho N \, \mathrm{d}V \tag{6}$$

$$C^e = \int_{V^e} N^T \mu N \, \mathrm{d}V \tag{7}$$

with $B = \partial N$, ∂ a linear operator, N the element shape functions, D the material stiffness matrix, V^e the volume of an element, ρ the material mass density, and μ the material damping factor. The calculation of an element stiffness, mass, or damping matrix consists of an integration over the volume of the element. This volume could be uncertain as a result of geometrical uncertainties in the input. The function to be integrated consists of factors based on the element shape functions and on mechanical properties. These mechanical properties could also be uncertain. Because all of the uncertainties are represented as fuzzy numbers, the calculation of these matrices is done using the concept of the α sublevels. Both the element volume and the mechanical properties are defined as interval inputs at each α sublevel. First, Eqs. (5–7) are substituted in Eqs. (2–4), respectively. Using the definition of the solution set as in Eq. (1), the interval system matrices $\boldsymbol{K}_\alpha$, $\boldsymbol{M}_\alpha$, and $\boldsymbol{C}_\alpha$ for this level yield

$$\boldsymbol{K}_\alpha = \left\{ K \mid (\exists \beta \in \boldsymbol{\beta}_\alpha)\left(K = \bigcup \int_{V^e(\beta)} B^T D(\beta) B \, \mathrm{d}V \right) \right\} \tag{8}$$

$$\boldsymbol{M}_\alpha = \left\{ M \mid (\exists \beta \in \boldsymbol{\beta}_\alpha)\left(M = \bigcup \int_{V^e(\beta)} N^T \rho(\beta) N \, \mathrm{d}V \right) \right\} \tag{9}$$

$$\boldsymbol{C}_\alpha = \left\{ C \mid (\exists \beta \in \boldsymbol{\beta}_\alpha)\left(C = \bigcup \int_{V^e(\beta)} N^T \mu(\beta) N \, \mathrm{d}V \right) \right\} \tag{10}$$

with β the vector $[\beta_1, \ldots, \beta_m]$ containing m uncertain parameters of the input model. For a given α sublevel each uncertainty β_i is bounded to its interval $\boldsymbol{\beta}_{i_\alpha}$, and $\boldsymbol{\beta}_\alpha = [\boldsymbol{\beta}_{1_\alpha}, \ldots, \boldsymbol{\beta}_{m_\alpha}]$.

3. Calculation of the Analysis Results

The analysis is performed by transforming the classical deterministic solution steps to the domain of interval arithmetic. For every α sublevel the solution set described in formula (1) is calculated, with $\mathcal{F}$ describing the solution procedure for the specific analysis. In literature[10] this is referred to as the *unified solution set*, defined as

$$\boldsymbol{y}_{\mathrm{KMC}_\alpha} = \{ y \mid (\exists K \in \boldsymbol{K}_\alpha)(\exists M \in \boldsymbol{M}_\alpha)(\exists C \in \boldsymbol{C}_\alpha)(y = \mathcal{F}(K, M, C)) \} \tag{11}$$

In the calculation of the classical solution set as in Eq. (11), the selection of a deterministic matrix A inside an interval matrix $\boldsymbol{A}$ is done by selecting all elements a_{ij} of the deterministic matrix such that $a_{ij} \in \boldsymbol{a}_{ij}$. All elements are selected independently from one another. Therefore, the solution set (11) considers the uncertainty on each element of the system matrices independently. This does not agree with reality because the elements of these matrices are calculated from common physical properties. Model properties like Young's modulus or material density are uncertain, but they are constant for the entire model. They cause element dependencies inside a system matrix. Geometrical model properties cause element relationships between the different system matrices. As a result, this solution set overestimates the realistic uncertainty on the result.

C. Generalized FFE Method

The generalized approach addresses the overestimation inherent to the classical approach as explained in Sec. II.B.3. This means that an exact calculation of the generalized solution set should yield the exact realistic interval on the result of the analysis. For this approach the model definition is entirely equivalent to the classical approach as discussed in Sec. II.B.1. The analysis however is directly performed on the related system matrices. This paper introduces the generalized unified solution set defined as

$$\boldsymbol{y}_{\beta_\alpha} = \{ y \mid (\exists \beta \in \boldsymbol{\beta}_\alpha)(y = \mathcal{F}(K(\beta), M(\beta), C(\beta))) \} \tag{12}$$

This approach combines the assembly of the system matrices and the calculation of the results in one solution set. As such, it incorporates the dependency of the system matrices on the uncertain input parameters directly into the analysis. The uncertainties in the system matrices are correlated through the uncertain input parameters. Therefore it describes the exact realistic range of the uncertainty on the analysis result.

D. Illustration of the Classical and Generalized Approach

This section illustrates both the classical and generalized approaches for the eigenvalue range calculation of an undamped structure.

1. Classical and Generalized Eigenvalue Problem

For the classical approach the eigenvalue solution set at an α sublevel equals

$$\boldsymbol{\lambda}_{\mathrm{KM}_\alpha} = \{ \lambda \mid (\exists K \in \boldsymbol{K}_\alpha)(\exists M \in \boldsymbol{M}_\alpha)(K\phi = \lambda M \phi) \} \tag{13}$$

with λ the analyzed eigenvalue and $\phi = [\phi_1, \ldots, \phi_n]$ the corresponding eigenvector. A number of analytical procedures exist for the calculation of the exact bounds on this classical solution set.[11–14]

For the generalized approach the solution set equals

$$\boldsymbol{\lambda}_{\beta_\alpha} = \{ \lambda \mid (\exists \beta \in \boldsymbol{\beta}_\alpha)(K(\beta)\phi = \lambda M(\beta)\phi) \} \tag{14}$$

The bounds on $\boldsymbol{\lambda}_{\beta_\alpha}$ can only be derived through optimization using

$$\bar{\lambda}_{\beta_\alpha} = \max_{\beta \in \boldsymbol{\beta}_\alpha} (\lambda) \tag{15}$$

$$\underline{\lambda}_{\beta_\alpha} = \min_{\beta \in \boldsymbol{\beta}_\alpha} (\lambda) \tag{16}$$

The optimization is easy if analytical expressions for the eigenvalue sensitivities to the input parameters are available. If not, more advanced optimization strategies should be applied.

2. Numerical Example

The numerical example consists of a system of four masses connected with four springs, as shown in Fig. 2. All values for the stiffnesses and masses are uncertain and mutually uncorrelated. The membership functions for the uncertainties are triangular. Table 1 defines the membership functions by specifying the top of the triangular function ($\alpha = 1$) and the interval at the bottom ($\alpha = 0$). Units are in the meter/kilogram/second (MKS) convention.

The results of both the classical and the generalized FFEM for the sublevel at $\alpha = 0$ are summarized in Table 2. The second column in this table refers to the eigenfrequency of the deterministic

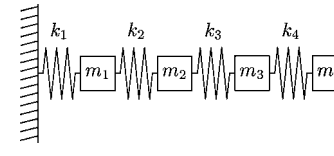

Fig. 2 Model for numerical analysis.

Table 1 Fuzzy properties of the numerical example

Uncertain parameter	Value at $\alpha = 1$	Interval at $\alpha = 0$
k_1, N/m	1025	[1000, 1050]
k_2, N/m	1575	[1550, 1600]
k_3, N/m	3025	[3000, 3050]
k_4, N/m	2325	[2300, 2350]
m_1, kg	5.5	[4, 7]
m_2, kg	13	[11, 15]
m_3, kg	9.5	[8, 11]
m_4, kg	17	[15, 19]

Table 2 Results of the classical and the generalized approach for the eigenfrequencies of the numerical example at $\alpha = 0$

Eigenfrequency	Reference model	Classical FFEM	Generalized FFEM
1	0.576	[0.392, 0.752]	[0.534, 0.628]
2	2.114	[1.932, 2.343]	[1.952, 2.317]
3	3.629	[3.234, 4.194]	[3.237, 4.192]
4	4.549	[4.196, 5.021]	[4.196, 5.021]

model at $\alpha = 1$. The classical solution sets result from application of Chen's method.[11] The generalized solution sets are the result of an optimization procedure.

The results for the first eigenfrequency indicate that the exact uncertainty interval given by the generalized solution set is much narrower than the classical solution set. This means that there is a significant overestimation of the uncertainty on the first eigenfrequency when using the classical approach. However, the computation of the classical solution is much faster since the bounds on the classical solution set (13) can be expressed analytically. This clearly illustrates that choosing between the classical and generalized approach involves a tradeoff between the size of the overestimation on the uncertainty and the computational effort. For the fourth frequency there is no difference between the classical and generalized solution set. This is because the stiffness and mass matrix selected independently by the classical method are the result of the combination of input uncertainties, which optimizes the eigenvalue. These matrices are by definition also the result of the generalized approach.

E. Computational Aspects of the Classical and Generalized FFE Approach

1. Computing the Exact Classical and Generalized Solution Set

The computation strategy for the exact classical solution set (11) depends on the considered type of analysis represented by $\mathcal{F}(K, M, C)$. For simple procedures like the eigenvalue problem, analytical procedures are available to calculate the exact bounds on the classical solution set. For more complex types of analyses, the exact bounds on the classical solution set cannot be expressed analytically. For these cases the only possibility to obtain the exact bounds is through a constrained optimization strategy. The optimization is performed using the elements of the system matrices as input variables and the analysis function $\mathcal{F}(K, M, C)$ as a goal function. Because the result is intended for design validation, the global minimum and maximum are required in order to include the worst-case scenario. For complex analyses this may be a cumbersome task because all matrix elements should be treated as independent input variables for the optimization.

So far, no analytical procedure exists to compute the exact generalized solution set (12) for any kind of analysis. The bounds of the set can only be computed through a constrained optimization problem on $\mathcal{F}(\beta)$. The global optimization is only possible if the sensitivity of the analysis result to the input uncertainties can be expressed analytically. This is only true for simple analyses like the eigenvalue problem. For more complex analyses the occurrence of local optima complicates the exact solution of the optimization.

2. Approximating the Classical and Generalized Solution Set

If there is no analytical expression for the bounds on the classical or generalized solution set and the optimization strategy fails, the exact solution set can be approximated. Two approximate methods are applicable for both the classical and the generalized approach.

The first method consists of translating all steps of a deterministic solution procedure of the considered analysis to interval arithmetic. This means that every operation of the deterministic solution procedure is replaced by its corresponding operation in interval arithmetic. The solution procedure can be any algorithm that performs the deterministic analysis. Each step during the algorithm is performed as an isolated interval operation. A small example illustrates this principle. Suppose the analysis consists of a simple division:

$$\mathcal{F}(a) = (a + 1)/a \tag{17}$$

Consider the classical solution set

$$\boldsymbol{y}_a = \{y \mid (a \in [1, 2])(y = (a + 1)/a)\} \tag{18}$$

Suppose that the solution strategy consists of two steps: the computation of the interval in the numerator and denominator in the first step and the division of both intervals in the second step. Applying this strategy results in the division of [2, 3] by [1, 2], which yields [1, 3]. However, after simplification of $\mathcal{F}(a)$ to $1 + 1/a$ the exact range of this solution set is $[\frac{3}{2}, 2]$. This indicates that this strategy overestimates the uncertainty on the analysis result. This phenomenon occurs when the same input uncertainties are present in multiple steps of the solution procedure. It is clear that the size of the overestimation depends on the choice of the deterministic solution procedure. However, because this approximation always overestimates the solution set it is safe for design validation. If this solution strategy is applied to the generalized solution set and the first step of the proposed solution strategy is the calculation of the system matrices, the resulting approximation is identical to the classical solution set.

A second method for this approximation is the vertex method.[15] The results for all possible combinations of boundary values on the input uncertainties are computed. The bounds on the exact generalized solution set are approximated taking the upper and lower limits of all of these results. A small example illustrates that this method does not ensure an inclusion of the exact solution set. Consider the solution set

$$\boldsymbol{y}_a = \{y \mid (a \in [0, 2])(y = (a - 1)^2)\} \tag{19}$$

The vertex solutions resulting from substituting 0 and 2 in the function are both 1. However, the exact range of the solution set is [0, 1]. Therefore, this method is not safe for design validation because the analyzed input boundary combinations do not necessarily include the global extremities of the goal function.

III. Application of the FFE Method for FRF Calculations

The remainder of this paper now considers the FRF calculation of an uncertain FE model. It describes a method for the calculation of a safe approximation of the generalized solution set, which is not based on the calculation of the system matrices but on the modal superposition principle. It overestimates the exact generalized solution set and is therefore safe for design validation.

A. Problem Definition

The calculation of the interval solution set for the analysis of uncertain vibrations was first analyzed by Elishakoff and Duan.[16] The interval solution of the basic FRF equation is the core of the FFEM for FRF calculations. This equation is based on the dynamic equilibrium

$$KX + C\dot{X} + M\ddot{X} = F \tag{20}$$

with K, C, and M, respectively the stiffness, damping, and mass matrices; X the displacement vector; and F the nodal forces vector. This work focuses on the FRF of undamped structures. The FRF is calculated using the matrix equation

$$(K - \omega^2 M)X = F \tag{21}$$

The FRF between node j and node k of an FE model is obtained taking the jth component of X satisfying Eq. (21) with

$$F = F_k = \begin{bmatrix} 0 \\ \vdots \\ 1 \\ \vdots \\ 0 \end{bmatrix} \rightarrow k\text{th row} \tag{22}$$

In the context of the classical FFEM, Eq. (21) is solved for each α sublevel using interval matrices for the stiffness and mass matrix. The classical solution set for the FRF between node j and k equals

$$\underline{\overline{\mathrm{FRF}_{jk}(\omega)}}_{\mathrm{KM}_\alpha} = \{X(j) \mid (\exists K \in \boldsymbol{K}_\alpha)(\exists M \in \boldsymbol{M}_\alpha)((K - \omega^2 M)X = F_k)\} \tag{23}$$

The calculation of the classical solution set (23) is equivalent to solving a system of linear interval equations. Recent research indicates that this is NP hard. This means that no efficient algorithm exists to calculate the exact bounds on this solution set within reasonable time. Analytical procedures are developed to construct approximate solution sets for this problem,[10,17–19] but none of these have proved to be efficient on large models. Therefore, the current work introduces a procedure for the calculation of a safe approximation of the generalized unified solution set

$$\underline{\overline{\mathrm{FRF}_{jk}(\omega)}}_{\beta_\alpha} = \{X(j) \mid (\exists \beta \in \boldsymbol{\beta}_\alpha)((K(\beta) - \omega^2 M(\beta))X = F_k)\} \tag{24}$$

The exact solution of Eq. (24) is commonly referred to as the envelope FRF.

B. Solution Strategy

This section indicates how the solution set (24) can be rewritten and safely approximated using the modal superposition principle. The modal superposition principle states that considering all n modes of a model, the FRF between node j and k equals

$$\mathrm{FRF}_{jk}(\omega) = \frac{X_j(\omega)}{F_k(\omega)} \tag{25}$$

$$= \sum_{i=1}^{n} \frac{\phi_{i_k}\phi_{i_j}}{\phi_i^T K \phi_i - \omega^2 \phi_i^T M \phi_i} \tag{26}$$

with $\phi_i = [\phi_{i_1}, \ldots, \phi_{i_n}]^T$ the ith eigenvector satisfying $K\phi_i = \lambda_i M \phi_i$. Simplification of Eq. (26) yields

$$\mathrm{FRF}_{jk}(\omega) = \sum_{i=1}^{n} \frac{1}{\hat{k}_i - \omega^2 \hat{m}_i} \tag{27}$$

with $\hat{k}_i$ and $\hat{m}_i$ the normalized modal parameters

$$\hat{k}_i = \frac{\phi_i^T K \phi_i}{\phi_{i_j}\phi_{i_k}} \tag{28}$$

$$\hat{m}_i = \frac{\phi_i^T M \phi_i}{\phi_{i_j}\phi_{i_k}} \tag{29}$$

Further, a mode i for which the normalized modal parameters $\hat{k}_i$ and $\hat{m}_i$ are both positive is referred to as a *positive mode*. A mode for which the normalized modal parameters $\hat{k}_i$ and $\hat{m}_i$ are both negative is referred to as a *negative mode*.

Using the modal superposition principle and the preceding definitions, the exact generalized solution set (24) equals

$$\underline{\overline{\mathrm{FRF}_{jk}(\omega)}}_{\beta_\alpha} = \left\{ \left(\sum_{i=1}^{n} \frac{1}{\hat{k}_i(\beta) - \omega^2 \hat{m}_i(\beta)} \right) \middle| \times (\exists \beta \in \boldsymbol{\beta}_\alpha)(K(\beta)\phi = \lambda M(\beta)\phi) \right\} \tag{30}$$

with $\phi = [\phi_1, \ldots, \phi_n]$ and $\lambda = \mathrm{diag}(\lambda_i)$. The normalized modal parameters depend on the uncertain parameters through the model properties incorporated in K and M and their corresponding eigenvectors as expressed in Eqs. (28) and (29).

The following set theoretic theorem is applied:

Theorem 1. With the preceding notations, given f_1 and f_2 are arbitrary functions of the parameters β_i, each of which is bounded to its interval $\boldsymbol{\beta}_i$, it can be shown that

$$\{(f_1(\beta) + f_2(\beta)) \mid (\exists \beta \in \boldsymbol{\beta})\} \subseteq \{f_1(\beta) \mid (\exists \beta \in \boldsymbol{\beta})\} \oplus \{f_2(\beta) \mid (\exists \beta \in \boldsymbol{\beta})\} \tag{31}$$

with $\oplus$ for general sets $\boldsymbol{x}$ and $\boldsymbol{y}$ defined as

$$\boldsymbol{x} \oplus \boldsymbol{y} = \{x + y \mid (\exists x \in \boldsymbol{x})(\exists y \in \boldsymbol{y})\} \tag{32}$$

Proof: The summation on the right-hand side of Eq. (31) considers the parameters for both functions independently, whereas the left-hand set results from considering equal values for the parameters in both functions. Therefore, the left-hand set is a subset of the right-hand set. □

Applying Theorem 1 on Eq. (30) yields

$$\underline{\overline{\mathrm{FRF}_{jk}(\omega)}}_{\beta_\alpha} \subseteq \bigoplus_{i=1}^{n} \left\{ \frac{1}{\hat{k}_i(\beta) - \omega^2 \hat{m}_i(\beta)} \middle| \times (\exists \beta \in \boldsymbol{\beta}_\alpha)(K(\beta)\phi = \lambda M(\beta)\phi) \right\} \tag{33}$$

The inequality in Eq. (33) indicates that the summation of the envelope FRF of each individual mode results in a safe approximation of the exact total envelope FRF:

$$\underline{\overline{\mathrm{FRF}_{jk}(\omega)}}_{\beta_\alpha} \subseteq \bigoplus_{i=1}^{n} \underline{\overline{\mathrm{FRF}_{jk}(\omega)_i}}_{\beta_\alpha} \tag{34}$$

It is obvious that if safe approximations of each single mode envelope FRF expressed as

$$\underline{\underline{\overline{\overline{\mathrm{FRF}_{jk}(\omega)_i}}}}_{\beta_\alpha}$$

are available the following inequality also holds:

$$\underline{\overline{\mathrm{FRF}_{jk}(\omega)}}_{\beta_\alpha} \subseteq \bigoplus_{i=1}^{n} \underline{\underline{\overline{\overline{\mathrm{FRF}_{jk}(\omega)_i}}}}_{\beta_\alpha} \tag{35}$$

This means that we now have an expression for a safe approximation of the total envelope FRF using safe approximations on all single mode envelope FRFs. The following section describes how these safe approximations of all single mode envelope FRFs are calculated. For the sake of clarity, the index α is omitted in the remainder of the paper, assuming that everything accounts for the interval analysis on each α sublevel.

C. Safe Single Mode Envelope FRF Approximation

1. *Exact Single Mode Envelope FRF*

First, the eigenfrequency range of a mode is introduced. It is defined as

$$\boldsymbol{\Omega}_{i_\beta} = \left\{ \sqrt{\lambda_i} \,\middle|\, (\exists \beta \in \boldsymbol{\beta})(K(\beta)\phi_i = \lambda_i M(\beta)\phi_i) \right\} \tag{36}$$

This is the generalized solution set of the eigenvalue analysis. This generalized solution set can only be derived through optimization as discussed in Sec. II.D.1:

$$\overline{\Omega_{i\beta}} = \max_{\beta \in \boldsymbol{\beta}} \sqrt{\lambda_i} \tag{37}$$

$$\underline{\Omega_i}_{\beta} = \min_{\beta \in \boldsymbol{\beta}} \sqrt{\lambda_i} \tag{38}$$

The exact single mode envelope FRF is defined as

$$\underline{\overline{\mathrm{FRF}_{jk}(\omega)_i}}_{\beta} = \left\{1\Big/\left(\hat{k}_i(\beta) - \omega^2\hat{m}_i(\beta)\right) \Big| \times (\exists\beta \in \beta)(K(\beta)\phi_i = \lambda_i M(\beta)\phi_i)\right\} \quad (39)$$

This expression basically is the inversion of the set of possible values of the denominator. This denominator set is different for each considered frequency because it is a function of ω. To calculate the set resulting from the inversion, the extended Kahan arithmetic[18] is applied. This is an extension to the definition of a classical interval division for division by a zero-containing interval. It states that the set resulting from the inversion of an interval $\boldsymbol{a} = [\underline{a}, \bar{a}]$ equals

$$[1/\bar{a}, 1/\underline{a}] \qquad \text{if} \qquad 0 \notin [\underline{a}, \bar{a}] \quad (40)$$

$$[-\infty, 1/\underline{a}] \cup [1/\bar{a}, +\infty] \qquad \text{if} \qquad 0 \in [\underline{a}, \bar{a}] \quad (41)$$

For a single mode FRF the denominator interval includes zero for frequencies that are within the eigenfrequency range (36) of the mode because, by definition, $\lambda_i = \hat{k}_i/\hat{m}_i$. This means that the calculation of Eq. (39) has to distinguish between frequencies within the eigenfrequency range and those outside the eigenfrequency range. The following procedure is introduced:

1) Calculate

$$\underline{\mathrm{FRF}_{jk}(\omega)_i}_{\beta} = 1\Big/\max_{\beta\in\beta}\left(\hat{k}_i - \omega^2\hat{m}_i\right) \quad (42)$$

$$\overline{\mathrm{FRF}_{jk}(\omega)_{i\beta}} = 1\Big/\min_{\beta\in\beta}\left(\hat{k}_i - \omega^2\hat{m}_i\right) \quad (43)$$

2) Calculate the eigenfrequency range $\boldsymbol{\Omega}_{i_\beta}$ for the current mode

3) Define the single mode envelope FRF using

$$\underline{\overline{\mathrm{FRF}_{jk}(\omega)_i}}_{\beta} = \left[\underline{\mathrm{FRF}_{jk}(\omega)_i}_{\beta}, \overline{\mathrm{FRF}_{jk}(\omega)_{i\beta}}\right] \qquad \text{for} \qquad \omega \notin \boldsymbol{\Omega}_{i\beta} \quad (44)$$

$$= \left[-\infty, \overline{\mathrm{FRF}_{jk}(\omega)_{i\beta}}\right] \cup \left[\underline{\mathrm{FRF}_{jk}(\omega)_i}_{\beta}, +\infty\right] \qquad \text{for} \qquad \omega \in \boldsymbol{\Omega}_{i\beta} \quad (45)$$

Figure 3 indicates the difference between the resulting sets for frequencies inside the eigenfrequency range (ω_{in}) and those outside the eigenfrequency range (ω_{out}). It also indicates that the preceding procedure applies for both negative and positive modes.

2. Single Mode Envelope FRF Approximation

The preceding section illustrates how the exact boundaries on the single mode envelope FRF can be computed. The core of this procedure is the optimization of the denominator of the single mode frequency response function in Eqs. (42) and (43). An exact solution would require an indefinite number of optimizations because a continuous frequency domain is considered. From Eq. (35) we know that the addition of safe approximations of each single mode envelope FRF results in a safe approximation of the total envelope FRF. Therefore, safe approximations of the optimization in Eqs. (42) and (43) will suffice. This is equivalent to computing safe approximations $\overline{\overline{\mathcal{F}}}$ and $\underline{\underline{\mathcal{F}}}$ for the goal function $\mathcal{F}(\omega) = [\hat{k}_i(\beta) - \omega^2\hat{m}_i(\beta)]$ satisfying

$$\overline{\overline{\mathcal{F}}}(\omega) \geq \overline{\mathcal{F}}(\omega) = \max_{\beta\in\beta}\left[\hat{k}_i(\beta) - \omega^2\hat{m}_i(\beta)\right] \quad (46)$$

$$\underline{\underline{\mathcal{F}}}(\omega) \leq \underline{\mathcal{F}}(\omega) = \min_{\beta\in\beta}\left[\hat{k}_i(\beta) - \omega^2\hat{m}_i(\beta)\right] \quad (47)$$

for $\omega \in [0, \infty]$. The safe approximations on this goal function are then inverted in order to obtain safe approximations on the single mode envelope FRF, expressed as

$$\underline{\underline{\mathrm{FRF}_{jk}(\omega)_i}}_{\beta} = 1/\overline{\overline{\mathcal{F}}}(\omega) \quad (48)$$

$$\overline{\overline{\mathrm{FRF}_{jk}(\omega)_{i\beta}}} = 1/\underline{\underline{\mathcal{F}}}(\omega) \quad (49)$$

The eigenfrequency range corresponding to the approximate optimization of the goal function $\mathcal{F}$ yields $[\underline{\underline{\Omega_i}}_{\beta}, \overline{\overline{\Omega_{i\beta}}}]$ with

$$\underline{\underline{\Omega_i}}_{\beta} = [\omega^* \mid \underline{\underline{\mathcal{F}}}(\omega^*) = 0] \quad (50)$$

$$\overline{\overline{\Omega_{i\beta}}} = [\omega^* \mid \overline{\overline{\mathcal{F}}}(\omega^*) = 0] \quad (51)$$

for positive modes and

$$\underline{\underline{\Omega_i}}_{\beta} = [\omega^* \mid \overline{\overline{\mathcal{F}}}(\omega^*) = 0] \quad (52)$$

$$\overline{\overline{\Omega_{i\beta}}} = [\omega^* \mid \underline{\underline{\mathcal{F}}}(\omega^*) = 0] \quad (53)$$

for negative modes. The lower and upper bound on the eigenfrequency are associated to, respectively, $\overline{\mathrm{FRF}_{jk}(\omega)_i}$ and $\underline{\mathrm{FRF}_{jk}(\omega)_i}$ for positive modes and vice versa for negative modes, as can be seen from Fig. 3. Therefore, the approximate eigenfrequency range distinguishes between positive and negative modes. It can easily be shown that this eigenfrequency range is an outer approximation of the exact generalized solution set of Eq. (36). Corresponding to Eqs. (44) and (45), the approximate single mode envelope FRF now equals

$$\underline{\underline{\overline{\mathrm{FRF}_{jk}(\omega)_i}}}_{\beta} = \left[\underline{\underline{\mathrm{FRF}_{jk}(\omega)_i}}_{\beta}, \overline{\overline{\mathrm{FRF}_{jk}(\omega)_{i\beta}}}\right] \qquad \text{for} \qquad \omega \notin \left[\underline{\underline{\Omega_i}}_{\beta}, \overline{\overline{\Omega_{i\beta}}}\right] \quad (54)$$

$$= \left[-\infty, \overline{\overline{\mathrm{FRF}_{jk}(\omega)_{i\beta}}}\right] \cup \left[\underline{\underline{\mathrm{FRF}_{jk}(\omega)_i}}_{\beta}, +\infty\right] \qquad \text{for} \qquad \omega \in \left[\underline{\underline{\Omega_i}}_{\beta}, \overline{\overline{\Omega_{i\beta}}}\right] \quad (55)$$

The remainder of this section focuses on how to compute the safe approximate optimizations $\overline{\overline{\mathcal{F}}}(\omega)$ and $\underline{\underline{\mathcal{F}}}(\omega)$ of the goal function $\mathcal{F}$. The most straightforward approximate solution strategy is to perform the optimization in Eqs. (46) and (47) for a limited number of discrete frequencies, and construct $\overline{\overline{\mathcal{F}}}(\omega)$ and $\underline{\underline{\mathcal{F}}}(\omega)$ interpolating through the results of these discrete optimizations. To ensure that this interpolation results in a safe approximation for all intermediate frequencies, the following theorem is applied.

Theorem 2. With the preceding notations, given the exact optimized values of the goal function $\mathcal{F}(\omega)$ for two distinct values of ω:

$$\max_{\beta\in\beta}\mathcal{F}(\omega_\iota) = \overline{\mathcal{F}}_\iota, \qquad \min_{\beta\in\beta}\mathcal{F}(\omega_\iota) = \underline{\mathcal{F}}_\iota$$

$$\max_{\beta\in\beta}\mathcal{F}(\omega_{\iota+1}) = \overline{\mathcal{F}}_{\iota+1}, \qquad \min_{\beta\in\beta}\mathcal{F}(\omega_{\iota+1}) = \underline{\mathcal{F}}_{\iota+1}$$

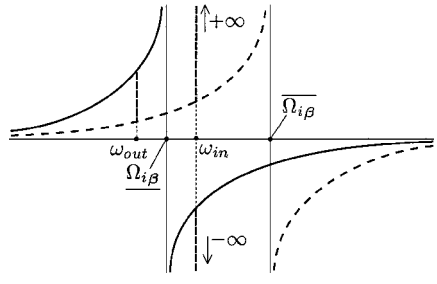

Positive mode

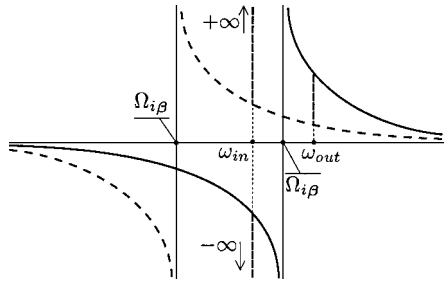

Negative mode

Fig. 3 Single mode envelope FRF: ——, $\overline{\mathrm{FRF}_{jk}(\omega)_{i\beta}}$ and - - -, $\underline{\mathrm{FRF}_{jk}(\omega)_i}_{\beta}$

with $\omega_\iota < \omega_{\iota+1}$, it can be shown that, for all $\omega^* \in [\omega_\iota, \omega_{\iota+1}]$,

$$\overline{\mathcal{F}}(\omega^*) \le \frac{\left(\omega_{\iota+1}^2 - \omega^{*2}\right)\overline{\mathcal{F}}_\iota + \left(\omega^{*2} - \omega_\iota^2\right)\overline{\mathcal{F}}_{\iota+1}}{\omega_{\iota+1}^2 - \omega_\iota^2}$$

$$\underline{\mathcal{F}}(\omega^*) \ge \frac{\left(\omega_{\iota+1}^2 - \omega^{*2}\right)\underline{\mathcal{F}}_\iota + \left(\omega^{*2} - \omega_\iota^2\right)\underline{\mathcal{F}}_{\iota+1}}{\omega_{\iota+1}^2 - \omega_\iota^2}$$

Proof. Only the first inequality is proven here. The proof of the second inequality follows the same procedure. If this theorem would be false, $\exists \omega^* \in [\omega_\iota, \omega_{\iota+1}]$:

$$\overline{\mathcal{F}}(\omega^*) > \frac{\left(\omega_{\iota+1}^2 - \omega^{*2}\right)\overline{\mathcal{F}}_\iota + \left(\omega^{*2} - \omega_\iota^2\right)\overline{\mathcal{F}}_{\iota+1}}{\omega_{\iota+1}^2 - \omega_\iota^2} \qquad (*)$$

Stating that $\overline{\mathcal{F}}(\omega^*)$ is achieved for $\beta = \beta^*$ and using the definition of $\mathcal{F}(\omega)$, this is equivalent to $\exists \hat{k}_i^* = \hat{k}_i(\beta^*), \hat{m}_i^* = \hat{m}_i(\beta^*)$:

$$\hat{k}_i^* - \omega^{*2}\hat{m}_i^* > \frac{\left(\omega_{\iota+1}^2 - \omega^{*2}\right)\overline{\mathcal{F}}_\iota + \left(\omega^{*2} - \omega_\iota^2\right)\overline{\mathcal{F}}_{\iota+1}}{\omega_{\iota+1}^2 - \omega_\iota^2}$$

Because $\overline{\mathcal{F}}_\iota$ and $\overline{\mathcal{F}}_{\iota+1}$ are optimal,

$$\hat{k}_i^* - \omega_\iota^2\hat{m}_i^* \le \overline{\mathcal{F}}_\iota, \qquad \hat{k}_i^* - \omega_{\iota+1}^2\hat{m}_i^* \le \overline{\mathcal{F}}_{\iota+1}$$

and therefore $\exists \hat{k}_i^* = \hat{k}_i(\beta^*), \hat{m}_i^* = \hat{m}_i(\beta^*)$:

$$\begin{aligned}
&\hat{k}_i^* - \omega^{*2}\hat{m}_i^* \\
&\quad > \frac{\left(\omega_{\iota+1}^2 - \omega^{*2}\right)\left(\hat{k}_i^* - \omega_\iota^2\hat{m}_i^*\right) + \left(\omega^{*2} - \omega_\iota^2\right)\left(\hat{k}_i^* - \omega_{\iota+1}^2\hat{m}_i^*\right)}{\omega_{\iota+1}^2 - \omega_\iota^2} \\
&\quad > \frac{\hat{k}_i^*\left(\omega_{\iota+1}^2 - \omega_\iota{}^2\right) - \hat{m}_i^*\left(\omega_{\iota+1}^2\omega^{*2} - \omega_\iota^2\omega^{*2}\right)}{\omega_{\iota+1}^2 - \omega_\iota^2} \\
&\quad > \hat{k}_i^* - \omega^{*2}\hat{m}_i^*
\end{aligned}$$

The preceding assumption $(*)$ must thus be invalid, and therefore the first inequality of this theorem is proven ad absurdum. □

This theorem shows that we can compose a safe approximation of the optimized goal function for all frequencies based on a limited number of exact optimizations spread over the frequency domain using a quadratic interpolation scheme.

3. *Graphical Interpretation*

A graphical representation of the single mode goal function clarifies why the quadratic interpolation procedure proposed in the preceding theorem ensures guaranteed upper and lower bounds on the exact interval. Consider a two-dimensional workspace in $\hat{k}_i$ and $\hat{m}_i$. In this workspace, for one given value of ω, the goal function is represented by a straight line, expressed as

$$\hat{k}_i - \omega^2\hat{m}_i = \mathcal{F}^* \qquad (56)$$

All $\hat{k}_i, \hat{m}_i$ pairs on this line represent structures with equal values $\mathcal{F}^*$ for the goal function. This value is graphically equivalent with the intersection point of the line represented by Eq. (56) and the $\hat{k}_i$ axis, as indicated in Fig. 4.

The $\hat{k}_i, \hat{m}_i$ combinations resulting from all possible combinations of input uncertainties β mark off a domain in the $\hat{k}_i, \hat{m}_i$ workspace:

$$\langle \hat{k}_i, \hat{m}_i \rangle_\beta = \{(\hat{k}_i(\beta), \hat{m}_i(\beta)) \mid (\beta \in \beta)\} \qquad (57)$$

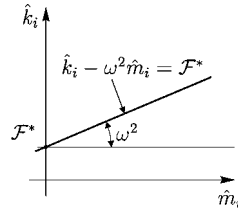

Fig. 4 Graphical interpretation of the goal function.

Optimizing the goal function for one specific value of ω is graphically equivalent to constructing both lines with a slope ω^2 tangent to $\langle \hat{k}_i, \hat{m}_i \rangle_\beta$ (one for the maximization, one for the minimization). The optimization for $\omega = 0 \to \infty$ is equivalent to circumscribing $\langle \hat{k}_i, \hat{m}_i \rangle_\beta$ by straight lines tangent to this domain with slopes ranging from 0 to 90 deg. Using this concept, the optimization is straightforward if an exact analytical description of the border of $\langle \hat{k}_i, \hat{m}_i \rangle_\beta$ is available. Because this is generally not the case, an approximate procedure based on a polygonal circumscription of $\langle \hat{k}_i, \hat{m}_i \rangle_\beta$ is introduced. The polygon consists of a limited number 2ν of lines tangent to $\langle \hat{k}_i, \hat{m}_i \rangle_\beta$. Because each border line of the polygon is tangent to $\langle \hat{k}_i, \hat{m}_i \rangle_\beta$, the goal functions represented by these lines are optimal at their corresponding frequencies $\omega_\iota, \iota = 1, \ldots, \nu$. Therefore, the borderlines are expressed as

$$\hat{k}_i - \omega_\iota^2\hat{m}_i = \overline{\mathcal{F}}_\iota, \qquad \iota = 1 \cdots \nu \qquad (58)$$

$$\hat{k}_i - \omega_\iota^2\hat{m}_i = \underline{\mathcal{F}}_\iota, \qquad \iota = 1 \cdots \nu \qquad (59)$$

These lines represent the result of steps 1 and 2 in the interpolation procedure. Now consider a frequency $\omega^* \in [\omega_\iota, \omega_{\iota+1}]$. The results of the exact optimization would be represented by lines with slope ω^{*2} tangent to $\langle \hat{k}_i, \hat{m}_i \rangle_\beta$. An approximation of the optimal goal function is calculated by constructing lines with this slope through the intersection point of the lines representing the optimized goal functions $\mathcal{F}(\omega_\iota)$ and $\mathcal{F}(\omega_{\iota+1})$. Because $\langle \hat{k}_i, \hat{m}_i \rangle_\beta$ is completely contained within the polygonal circumscription, this approximation is on the safe side of the exact (unknown) optimized goal function. This is illustrated in Fig. 5. In this figure $\overline{\mathcal{F}}(\omega^*)$ is unknown but safely overestimated by $\overline{\overline{\mathcal{F}}}(\omega^*)$, resulting from constructing a line with slope ω^{*2} through the intermediate corner point of the circumscribing polygon. The intermediate corner points are referred to as *interpolation points* and are symbolized by a triangle in each figure. Repeating this procedure for all intermediate frequencies results in an approximation of the optimized goal function using all corner points of the circumscribing polygon. This is mathematically equivalent to the quadratic interpolation in step 3 of the interpolation procedure. Figure 6 clarifies the graphical interpretation of the interpolation procedure for $\nu = 4$ with $\omega_1 = 0$ and $\omega_\nu = \infty$.

4. *Proposed Approximate Optimization Strategies*

This paper illustrates the single mode approximate optimization procedure using a strategy based on only two discrete optimizations: the corner method. Later, it is shown how the results of the exact eigenfrequency range calculation through optimization in Eqs. (37) and (38) add delimiters to $\langle \hat{k}_i, \hat{m}_i \rangle_\beta$. This results in the corner-eigenvalue method. The optimized vertex method, which is

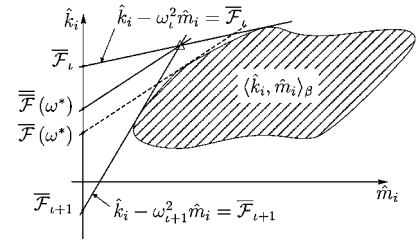

Fig. 5 Safe approximations using the circumscribing polygon.

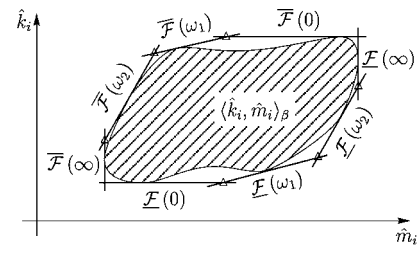

Fig. 6 Approximate circumscribing polygon.

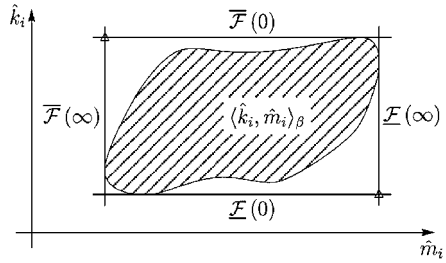

a) Corner method

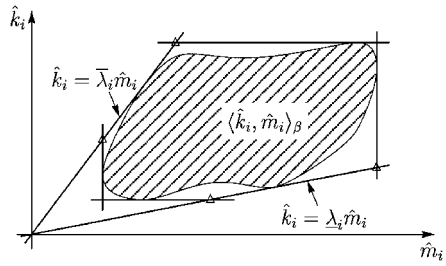

b) Corner-eigenvalue method

Fig. 7 Graphical interpretation of the proposed approximation strategies.

a safe extension of the classical vertex method, is considered as the reference for the comparison of the proposed methods.

The corner method creates a rectangular circumscription of $\langle \hat{k}_i, \hat{m}_i \rangle_\beta$ using the optimization of $\mathcal{F}(0)$ and $\mathcal{F}(\infty)$. From the definition of $\mathcal{F}(\omega)$, it is clear that this procedure involves the independent optimization of the normalized modal parameters

$$\underline{\mathcal{F}}(0) = \min_{\beta \in \beta} \hat{k}_i \tag{60}$$

$$\overline{\mathcal{F}}(0) = \max_{\beta \in \beta} \hat{k}_i \tag{61}$$

$$\underline{\mathcal{F}}(\infty) \leftrightarrow \max_{\beta \in \beta} \hat{m}_i \tag{62}$$

$$\overline{\mathcal{F}}(\infty) \leftrightarrow \min_{\beta \in \beta} \hat{m}_i \tag{63}$$

Figure 7a displays the resulting rectangular region. The upper-left-hand and lower-right-hand corners of this rectangle are the interpolation points.

The corner-eigenvalue method adds the results of the eigenvalue optimization as defined in Eqs. (37) and (38) to the rectangular area of the corner method. Because $\lambda_i = \hat{k}_i / \hat{m}_i$, the lines expressed as

$$\hat{k}_i = \overline{\lambda}_i \hat{m}_i \tag{64}$$

$$\hat{k}_i = \underline{\lambda}_i \hat{m}_i \tag{65}$$

represent lines with maximal and minimal slope through the origin of the $\hat{k}_i, \hat{m}_i$ workspace. These are new delimiters to the circumscription of $\langle \hat{k}_i, \hat{m}_i \rangle_\beta$ as indicated in Fig. 7b.

The optimized vertex method is a safe extension of the classical vertex method. The classical vertex method as described in Sec. II.E.2 produces a cloud of $(\hat{k}_i, \hat{m}_i)$ combinations using only the boundary values of each input interval. Because this method does not necessarily include global extremities, it does not ensure a circumscription of $\langle \hat{k}_i, \hat{m}_i \rangle_\beta$. To address this problem, discrete optimizations are performed for the frequencies represented by the slope of each border line of the area resulting from the vertex method. This method is safe, but requires an unknown number of optimizations.

D. Summation of the Single Mode Envelope FRF Approximations

The final step for the computation of the approximate total envelope FRF is executing the summation over all modes as indicated in Eq. (35):

$$\underline{\overline{\mathrm{FRF}_{jk}(\omega)}}_\beta = \bigoplus_{i=1}^{n} \underline{\overline{\mathrm{FRF}_{jk}(\omega)_i}}_\beta \tag{66}$$

Because the approximate single mode envelope FRF differs for frequencies within and outside the eigenfrequency range of each mode, the summation distinguishes between three subcases:

1) For frequencies outside every eigenfrequency range, all terms in the summation are of the form of Eq. (54), and therefore

$$\bigoplus_{i=1}^{n} \underline{\overline{\mathrm{FRF}_{jk}(\omega)_i}}_\beta = \left[\sum_{i=1}^{n} \underline{\mathrm{FRF}_{jk}(\omega)_i}_\beta , \sum_{i=1}^{n} \overline{\mathrm{FRF}_{jk}(\omega)_{i\beta}} \right] \tag{67}$$

2) For frequencies inside exactly one eigenfrequency range, one term in the summation is of the form of Eq. (55), and therefore

$$\bigoplus_{i=1}^{n} \underline{\overline{\mathrm{FRF}_{jk}(\omega)_i}}_\beta = \left[-\infty, \sum_{i=1}^{n} \overline{\mathrm{FRF}_{jk}(\omega)_{i\beta}} \right] \cup \left[\sum_{i=1}^{n} \underline{\mathrm{FRF}_{jk}(\omega)_i}_\beta , +\infty \right] \tag{68}$$

3) For frequencies inside two eigenfrequency ranges, two terms in the summation are of the form of Eq. (55), and therefore

$$\bigoplus_{i=1}^{n} \underline{\overline{\mathrm{FRF}_{jk}(\omega)_i}}_\beta = [-\infty, +\infty] \tag{69}$$

E. Algorithm

The algorithm for the calculation of a safe approximation for an envelope FRF is as follows.

1) For all modes do the following:

a) Define a grid in the frequency domain consisting of ν frequencies: $[\omega_1, \ldots, \omega_\nu]$.

b) Perform the exact optimization of the goal function $\mathcal{F} = \hat{k}_i - \omega^2 \hat{m}_i$ for these frequencies.

c) Compose an approximation for the optimized goal function $\overline{\overline{\mathcal{F}}}(\omega)$ and $\underline{\underline{\mathcal{F}}}(\omega)$ for all intermediate frequencies $\omega \in [\omega_1, \omega_\nu]$ using the quadratic interpolation scheme of theorem 2.

d) Calculate the safe boundaries on the single mode envelope FRF inverting $\overline{\overline{\mathcal{F}}}(\omega)$ and $\underline{\underline{\mathcal{F}}}(\omega)$.

e) Calculate safe approximations on the eigenfrequency bounds corresponding to $\overline{\overline{\mathcal{F}}}(\omega)$ and $\underline{\underline{\mathcal{F}}}(\omega)$ using Eqs. (50–53).

f) Calculate the safe approximation of the single mode envelope FRF using Eqs. (54) and (55).

2) Sum all single mode envelope FRF approximations using Eqs. (67–69).

The number of frequencies chosen in step 1a is proportional to the amount of work in step 1b, but inversely proportional to the size of the overestimation of each single mode envelope FRF. Therefore the choice of the frequency grid is a tradeoff between accuracy of the approximation and computational effort. Theorem 2 proves that step 1c in this procedure will result in guaranteed upper and lower bounds on the optimized goal function for all frequencies. Step 1e applied to the result of the corner-eigenvalue method results in the exact eigenfrequency bounds because the approximate optimized goal functions $\overline{\overline{\mathcal{F}}}(\omega)$ and $\underline{\underline{\mathcal{F}}}(\omega)$ equal zero for the exact bounds of the eigenvalues as can be seen from Fig. 7b.

IV. Numerical Example

The FFE method for FRF calculations is illustrated on the calculation of the FRF between masses 3 and 4 of the numerical example introduced in Sec. II.D.2. First, the different single mode envelope FRF approximation techniques are illustrated for the sublevel $\alpha = 0$. The resulting total envelope FRFs are compared at the same sublevel. To validate the interval analysis, the resulting boundaries are compared to the results of a Monte Carlo simulation assuming a uniform distribution over the interval. This Monte Carlo simulation does not represent the probabilistic analysis of the uncertain model, which in this case cannot be done because there is no information on the probability distributions of the uncertainties. It is only used to indicate the physical output domain of the interval analysis at the specific α-level, which enables the verification of the conservative

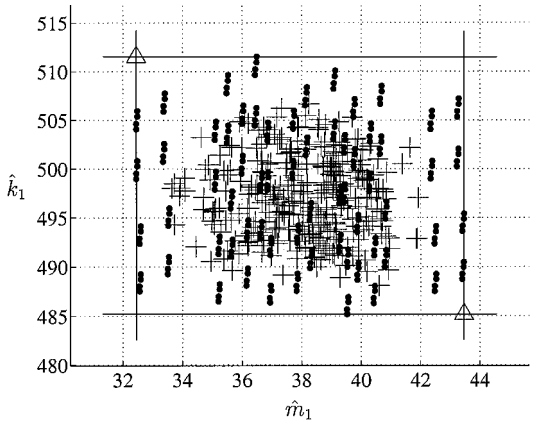

Corner method

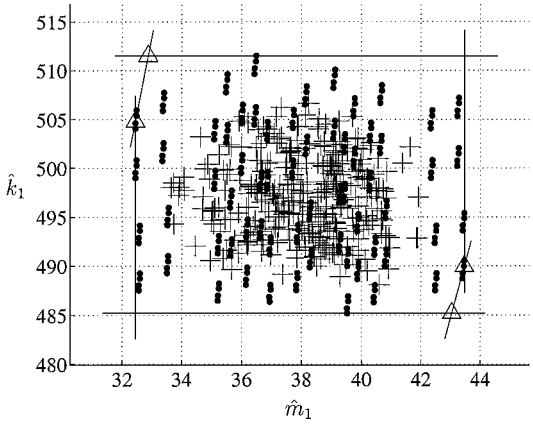

Corner-eigenvalue method

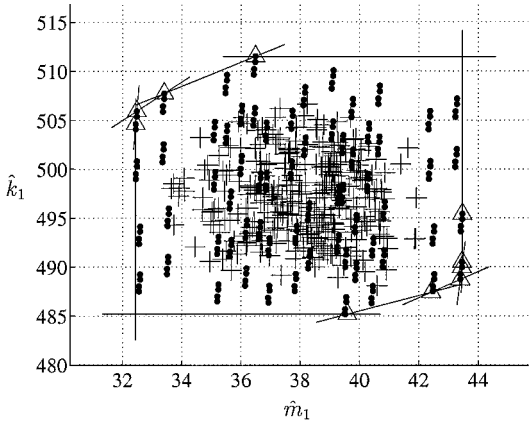

Optimized vertex method

Fig. 8 Comparison of $\langle \hat{k}_1, \hat{m}_1 \rangle_\beta$ for the three proposed methods: △, corner point of polygon used for quadratic interpolation; •, $(\hat{k}_1, \hat{m}_1)$ combinations from vertex method; and +, $(\hat{k}_1, \hat{m}_1)$ combinations from Monte Carlo simulation.

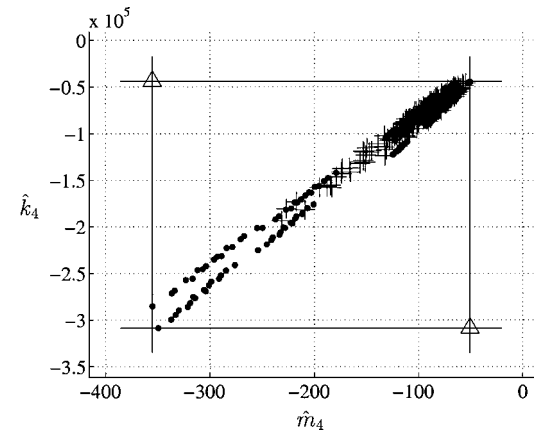

Corner method

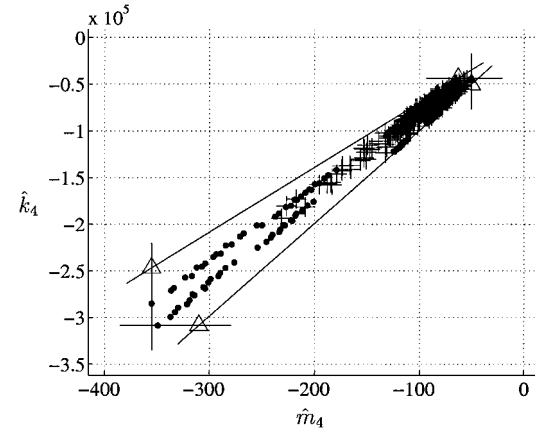

Corner-eigenvalue method

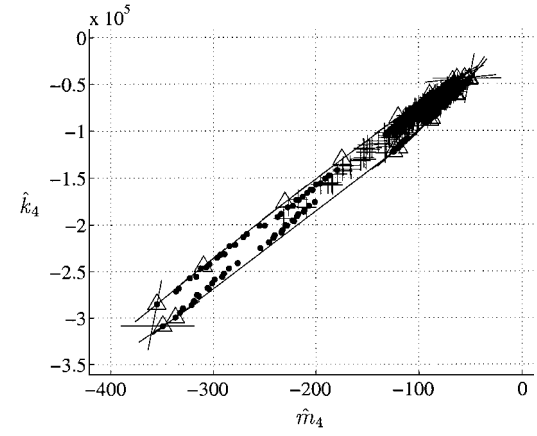

Optimized vertex method

Fig. 9 Comparison of $\langle \hat{k}_4, \hat{m}_4 \rangle_\beta$ for the three proposed methods: △, corner point of polygon used for quadratic interpolation; •, $(\hat{k}_4, \hat{m}_4)$ combinations from vertex method; and +, $(\hat{k}_4, \hat{m}_4)$ combinations from Monte Carlo simulation.

approximation. Finally, the fuzzy FRF is calculated by combining 11 α sublevels.

A. Single Mode Envelope FRF Approximation at $\alpha = 0$

Figure 8 compares the polygon for the three methods proposed in Sec. III.C.4 for the first mode of this model. They are plotted upon the $\hat{k}_1, \hat{m}_1$ pairs resulting from the vertex method (dots) and those resulting from 320 Monte Carlo samples using a uniform probability distribution over each interval at $\alpha = 0$ (crosses). The subsequent corner points of the polygon used for the quadratic interpolation are indicated with triangles. This figure indicates that for this mode the rectangular area of the corner method is a good approximation of $\langle \hat{k}_1, \hat{m}_1 \rangle_\beta$ because the $\hat{k}_1, \hat{m}_1$-pairs resulting from the vertex method describe a quasi rectangular area. Adding the eigenvalue delimiters or applying the optimized vertex method does not substantially decrease the size of the overestimation of $\langle \hat{k}_1, \hat{m}_1 \rangle_\beta$.

Figure 9 compares the polygon for the three methods proposed in Sec. III.C.4 for the fourth mode of this model. Again, they are plotted upon the $\hat{k}_4, \hat{m}_4$ pairs resulting from the vertex method (dots) and those resulting from 320 Monte Carlo samples using a uniform probability distribution over each interval (crosses). The subsequent corner points of the polygon used for the quadratic interpolation are indicated with triangles. This figure indicates that the $\langle \hat{k}_4, \hat{m}_4 \rangle_\beta$ circumscription of the corner method substantially overestimates the exact domain. Adding the results of the eigenvalue optimization results in a much closer circumscription. The optimized vertex method results in the closest circumscription.

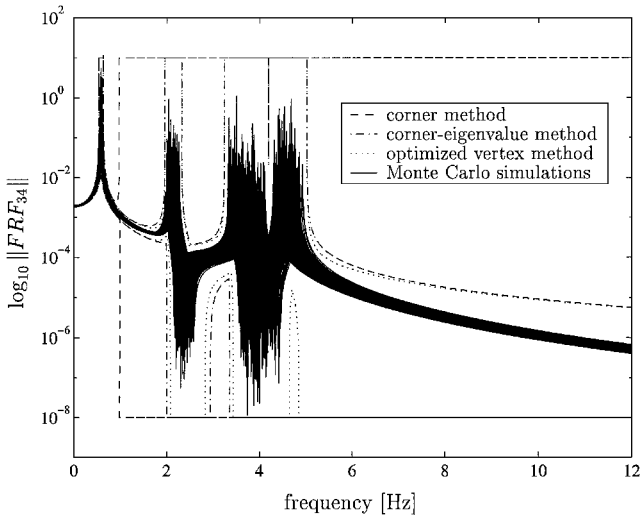

Fig. 10 Comparison of the resulting envelope FRF_{34} for the corner method, the corner-eigenvalue method, and the optimized vertex method with 320 Monte Carlo samples.

B. Total Envelope FRF at $\alpha = 0$

Figure 10 compares the resulting total FRFs for the three approximate optimization methods. The response ranges to infinity because an undamped structure is considered. Therefore, the logarithmic range has been cut off at 10^{-8} and 10^{1}. It is clear that the resulting envelope FRF of the corner method is only useful up to the first eigenfrequency. This is because of the fact that the corner method produced a good approximation of $\langle \hat{k}_1, \hat{m}_1 \rangle_\beta$, but failed to give a close approximation of $\langle \hat{k}_i, \hat{m}_i \rangle_\beta$ for the higher modes. The large overestimation for these modes is translated into an envelope FRF ranging from zero to infinity for the main part of the frequency region. Adding the eigenvalue optimization results makes the resulting envelope FRF much more useful compared to the corner method. The results of the optimized vertex method differ only slightly from those of the corner eigenvalue method. The total envelope FRFs resulting from 320 samples of a Monte Carlo simulation are plotted on top of the envelope FRF approximations. It is clear that, for this case, the bounds on the response are safe and the margin on the response between physical samples and predicted bounds is small.

C. Total Fuzzy FRF

Figure 11 gives a graphical interpretation of the fuzzy FRF between mass 3 and 4 resulting from the different approximate optimization strategies, combining 11 α sublevels.

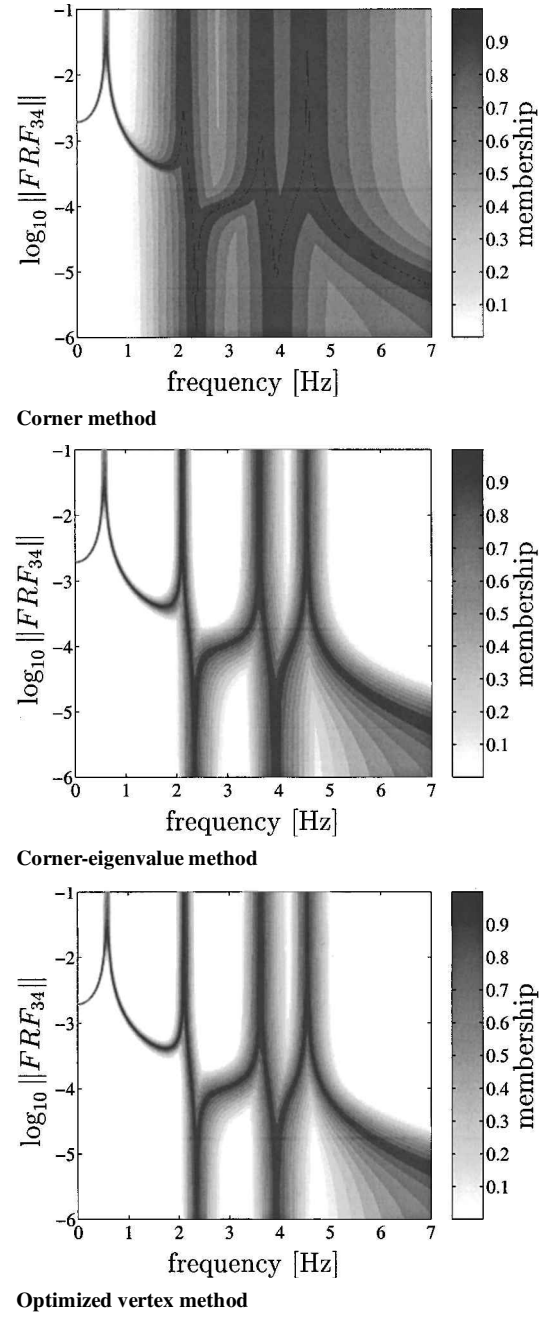

Fig. 11 Comparison of the fuzzy FRF_{34} for the three proposed methods.

V. Extension to Large-Scale FE Analysis

The preceding section indicates that the application of the proposed algorithm to an academic example results in a conservative approximation of the total envelope FRF. The applicability of the proposed method to more complex analyses depends on the performance of the algorithm of Sec. III.E for large-scale FE models. The algorithm basically is a sequence of analytical operations using the optimized goal function $\mathcal{F}(\omega)$ at the predefined frequency grid and in case of the corner-eigenvaluemethod the optimized eigenfrequencies. The performance of the algorithm depends mainly on the procedures to obtain these optimized values. Generally, the performance of an optimization procedure is influenced by two aspects: the evaluation time of the goal function (and if available its derivatives) and the convergence rate of the used optimization strategy.

In this case an eigenvalue analysis is necessary for each goal function evaluation. Therefore, the relative effect of the model size on the total computation time is equal to its relative effect on the eigenvalue analysis. However, the modal superposition principle enables us to reduce this effect. It is common practice to truncate the superposition to a limited number of modes, situated in the frequency domain of interest. This truncation will reduce the effect of the model size on the goal function evaluation because only a limited number of eigenvalues and corresponding eigenmodes are necessary. This would not have been possible if a direct solution strategy were chosen for the FRF calculation.

The convergence rate of large-scale optimization strategies mainly depends on the number of design variables, which affects the computation time exponentially. Therefore, we conclude that the number of design variables rather than the model size forms the most stringent limitation for the application of the algorithm to large-scale FE analysis.

VI. Conclusions

It has been shown that the classical FFE method inherently overestimates the uncertainty on the result of the FFE analysis. The generalized FFE approach theoretically describes the exact range of the uncertainty on the result of a FE analysis. Therefore, the generalized approach is preferred over the classical approach because its theoretical background is closer to reality. However, computation of the exact result of the generalized FFE analysis is hard because only optimization strategies are applicable. As an alternative, the uncertainty of a generalized FFE analysis can be safely approximated

using specific algorithms, as illustrated for the FRF calculation. The approximate optimization strategies described for this purpose are clearly a tradeoff between computational effort and accuracy of the result. The corner method needs four optimizations for each mode but fails to give a sufficiently narrow circumscription of the uncertainty on the total FRF. The results of the corner-eigenvalue method, which needs two extra optimizations on the eigenvalues for each mode, are much better and approach the results of the far more intensive optimized vertex method. Based on these conclusions, the corner-eigenvalue method is selected for further investigation.

References

[1]Contreras, H., "The Stochastic Finite-Element Method," *Computers and Structures*, Vol. 12, 1980, pp. 341–348.

[2]Haldar, A., and Mahadevan, S., *Reliability Assessment Using Stochastic Finite Element Analysis*, Wiley, New York, 2000.

[3]Székely, G., Pradlwarter, H., Schuller, G., Marchante, E., Diez, R., and Teichert, W., "A Detailed Scatter Analysis of the Structural Response of S/C's," *Proceedings of the European Conference on Spacecraft Structures, Materials and Mechanical Testing*, edited by B. Schürmann, ESA, Noordwijk, The Netherlands, 2000, pp. 605–610.

[4]Elishakoff, I., "Essay on Uncertainties in Elastic and Viscoelastic Structures: from A. M. Freudenthal's Criticisms to Modern Convex Modelling," *Computers and Structures*, Vol. 56, No. 6, 1995, pp. 871–895.

[5]Rao, S., and Sawyer, P., "Fuzzy Finite Element Approach for the Analysis of Imprecisely Defined Systems," *AIAA Journal*, Vol. 33, No. 12, 1995, pp. 2364–2370.

[6]Zadeh, L., "Fuzzy Sets," *Information and Control*, Vol. 8, 1965, pp. 338–353.

[7]Zadeh, L., "Fuzzy Sets as a Basis for a Theory of Possibility," *Fuzzy Sets and Systems*, Vol. 1, 1978, pp. 3–28.

[8]Dubois, D., and Prade, H., *Possibility Theory*, Plenum, New York, 1988.

[9]Civanalar, M., and Trussell, H., "Constructing Membership Functions Using Statistical Data," *Fuzzy Sets and Systems*, Vol. 18, 1986, pp. 1–13.

[10]Shary, S., "Algebraic Approach in the 'Outer Problem' for Interval Linear Equations," *Reliable Computing*, Vol. 3, 1997, pp. 103–135.

[11]Chen, S., Qiu, Z., and Song, D., "A New Method for Computing the Upper and Lower Bounds on Frequencies of Structures with Interval Parameters," *Mechanics Research Communications*, Vol. 22, No. 5, 1995, pp. 431–439.

[12]Dimarogonas, A., "Interval Analysis of Vibrating Systems," *Journal of Sound and Vibration*, Vol. 183, No. 4, 1995, pp. 739–749.

[13]El-Gebeily, M., Abu-Baker, Y., and Elgindi, M., "The Generalized Eigenvalue Problem for Tridiagonal Symmetric Interval Matrices," *International Journal on Control*, Vol. 72, No. 6, 1999, pp. 531–535.

[14]Teichert, W., and Székely, G., "Interval Prediction of Eigenvalues, Eigenvectors and Frequency Response Functions," *Advances in Safety and Reliability, Proceedings of the ESREL '97 International Conference on Safety and Reliability*, edited by C. G. Soares, Pergamon, Amsterdam, 1997, pp. 1331–1340.

[15]Dong, W., and Shah, H., "Vertex Method for Computing Function of Fuzzy Variables," *International Journal of Fuzzy Sets and Systems*, Vol. 24, 1987, pp. 65–78.

[16]Elishakoff, I., and Duan, D., "Application of Mathematical Theory of Interval Analysis to Uncertain Vibrations," *Proceedings of the 1994 National Conference on Noise Control Engineering*, edited by J. M. Cuschieri, S. A. L. Glegg, and D. M. Yeager, Inst. of Noise Control Engineering, Poughkeepsie, NY, 1994, pp. 519–524.

[17]Neumaier, A., *Interval Methods for Systems of Equations*, Cambridge Univ. Press, Cambridge, England, U.K., 1990.

[18]Shary, S., "On Optimal Solution of Interval Linear Equations," *SIAM Journal on Numerical Analysis*, Vol. 32, No. 2, 1995, pp. 610–630.

[19]Hansen, E., "Bounding the Solution of Interval Linear Equations," *SIAM Journal on Numerical Analysis*, Vol. 29, No. 5, 1992, pp. 1493–1503.

S. Saigal
Associate Editor